


Efficient Microwave Photon-to-Electron Conversion in a High-Impedance Quantum Circuit

O. Stanisavljević, J.-C. Philippe¹, J. Gabelli¹, M. Aprili, J. Estève¹, and J. Basset^{1*}
Université Paris-Saclay, CNRS, Laboratoire de Physique des Solides, 91405 Orsay, France

 (Received 11 January 2024; revised 7 May 2024; accepted 26 June 2024; published 16 August 2024)

We demonstrate an efficient and continuous microwave photon-to-electron converter with large quantum efficiency (83%) and low dark current. These unique properties are enabled by the use of a high kinetic inductance disordered superconductor, granular aluminium, to enhance light-matter interaction and the coupling of microwave photons to electron tunneling processes. As a consequence of strong coupling, we observe both linear and nonlinear photon-assisted processes where two, three, and four photons are converted into a single electron at unprecedentedly low light intensities. Theoretical predictions, which require quantization of the photonic field within a quantum master equation framework, reproduce well the experimental data. This experimental advancement brings the foundation for high-efficiency detection of individual microwave photons using charge-based detection techniques.

DOI: [10.1103/PhysRevLett.133.076302](https://doi.org/10.1103/PhysRevLett.133.076302)

Introduction—In the optical domain, the photoelectric effect is the method of choice to build single photon detectors covering a wide frequency spectrum with large quantum efficiency and low dark current [1]. Reducing the photon energy down to microwave frequencies (~ 10 GHz), while fulfilling the requirements for single photon detection, is experimentally challenging because of the absence of semiconducting or superconducting materials with a sufficiently low energy gap. Consequently, efficient single microwave photon detectors rely so far on alternate strategies using the circuit quantum electrodynamics toolbox, which has its own limitations [2–8]. Recently, experiments in hybrid circuits combining semiconducting quantum dots with high finesse microwave cavities have monitored photon-assisted tunneling processes using single electron charge detectors [9–13]. However, the conversion efficiency of the incoming photons into electrons remained low.

In this Letter, we demonstrate that photon-assisted quantum tunneling of quasiparticles in a voltage-biased superconducting tunnel junction, which has been known for a long time [14–20], can be pushed close to the limit where every incoming photon is converted into a tunneling electron. The impedance matching of the microwave mode to the tunnel junction is achieved by using a high impedance material, granular aluminum (grAl), which is a high kinetic inductance disordered superconducting material with interesting material properties [21–26]. We reach 83% quantum efficiency while keeping a low dark current (3.4×10^5 e/s) through the junction in the absence of incoming light. From a more fundamental perspective, our experiment addresses the question of photon-assisted

tunneling in the regime where a quantum description of the microwave signal is mandatory to reach a quantitative understanding of the process. Our work is complementary to previous works dealing with Cooper pairs tunneling in high impedance environments [27–32] and extends it to incoherent quasiparticle tunneling [33,34]. In particular, we observe high order processes where photon-assisted tunneling takes place through the absorption of two, three, and four photons, while remaining in the quantum regime, where the mean occupancy of the microwave mode is on the order of a few photons. The nonlinear power dependence of the tunneling current for these different processes allows us to obtain an absolute calibration of the incoming photon flux.

Principle of the experiment—The principle of the experiment is shown in Fig. 1. A dc-biased superconducting tunnel junction is connected to a quarter wavelength resonator made of grAl with a high characteristic impedance. The microwave photons that we aim to convert into electrons are fed to the resonator by a microstrip 50 Ω waveguide visible on the left of Fig. 1(a). The photon-assisted tunneling of one quasiparticle through the absorption of one photon from the resonator mode is energetically allowed if the bias voltage V satisfies $eV > 2\Delta - \hbar\omega$, where Δ is the superconducting gap and ω the frequency of the resonator [see Fig. 1(b)]. At low temperature, and in the absence of photons, no dc current flows through the junction if $eV < 2\Delta$. The working voltage range of the detector is therefore $2\Delta - \hbar\omega < eV < 2\Delta$, where the dark current is low and the one photon photon-assisted tunneling process is allowed. The probability that an incoming photon is absorbed and converted into an electron defines the detector quantum efficiency, which reaches unity when the coupling rate κ_c from the resonator to the waveguide

*Contact author: julien.basset@universite-paris-saclay.fr

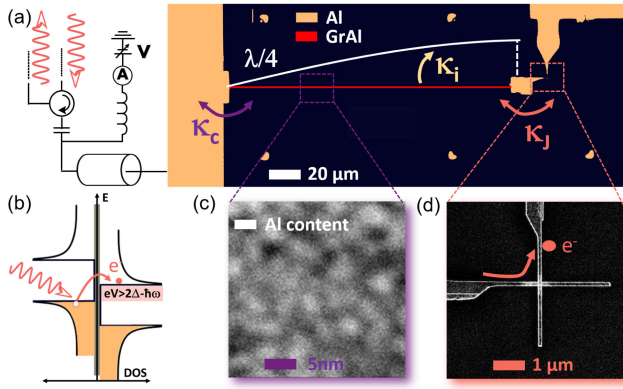


FIG. 1. Principle of the experiment. (a) Microscope image of the device and simplified schematic of the measurement setup. An incoming microwave photon is efficiently converted into an electron by coupling a waveguide to a high-impedance resonator (red). Efficient conversion is reached when the loss rate κ_j due to photon-assisted tunneling through the junction matches the coupling rate κ_c to the input waveguide. The quarter wavelength resonator is made out of granular aluminum; the junction is aluminium based. (b) Energy diagram (E, vertical axis) of the displaced superconducting density of states (DOS, horizontal axis) of the voltage biased superconducting tunnel junction and a sketch of the photon-assisted tunneling of quasiparticles. The bias voltage sets a frequency band in which photons can be absorbed, while no elastic current flows through the junction. (c) Chemical content sensitive transmission electron microscope image of a granular aluminum thin film. Brighter colors mean larger aluminium content. Darker areas have a stronger oxygen content. (d) Scanning electron microscope image of the superconducting tunnel junction.

matches the absorption rate κ_j due to the photon-assisted tunneling (PAT) process. This is equivalent to an impedance matching condition. Here, we have supposed for simplicity that other internal losses are negligible.

Below the gap, the PAT rate coming from single photon absorption [33,35–37] is given by

$$\kappa_j = \lambda^2 \exp(-\lambda^2) I(V + \hbar\omega/e)/e, \quad (1)$$

where the coupling constant $\lambda = \sqrt{\pi Z_C/R_K}$ is set by the ratio of the characteristic impedance of the mode Z_C to the quantum of resistance $R_K = h/e^2$ and $I(V)$ is the current voltage characteristic of the junction. In the experiment presented here, we designed the grAl resonator to reach $\lambda \sim 0.8$. The coefficient $\lambda^2 \exp(-\lambda^2)$ corresponds to the Franck-Condon matrix element $|\langle 0|D_\lambda|1\rangle|^2$, where D_λ is the displacement operator $\exp[i\lambda(a + a^\dagger)]$, which translates the charge degree of freedom of the resonator mode a by one electron [35]. Connecting the resonator to a 50Ω waveguide typically leads to a coupling rate $\kappa_c \sim 2\pi \times 80$ MHz (see Supplemental Material [38]).

A straightforward estimate based on Eq. (1) indicates that a junction with a resistance of about $1.5 \text{ M}\Omega$ fulfills the

impedance matching condition in the detector bias window [38]. This large value of the tunnel junction resistance is highly beneficial to reduce the elastic tunneling rate and therefore the dark current, which is a key figure of merit. In a conventional low-impedance resonator, the Franck-Condon factor $\lambda^2 \exp(-\lambda^2)$ would reduce the photon-assisted tunneling rate by approximately 2 orders of magnitude. The matching condition could still be reached, but with a much more transparent junction, which is detrimental in terms of dark current. Assuming a detector with a 200Ω characteristic impedance and the same bandwidth would require a tunnel resistance about $100 \text{ k}\Omega$. With a Dynes parameter of 10 neV [19], a subgap current of roughly 2 pA ($\approx 14 \text{ Me/s}$) is then expected at the operating voltage. The sample shown in Fig. 1 is fabricated via a three-step process using standard e-beam and optical lithography techniques. It is then mounted in a dilution fridge with a base temperature of 20 mK with a measurement circuit, which allows us to dc-bias the tunnel junction, feed microwaves, and measure the sample microwave reflection S_{11} . The measured resonator has a characteristic impedance of $5.1 \text{ k}\Omega$ ($\lambda = 0.79$), and the normal state resistance of the junction, obtained by triple oxidation, is $1.53 \text{ M}\Omega$ [38].

Microwave spectroscopy—We show in Fig. 2(a) a color map of the reflection coefficient $|S_{11}|^2$ of the resonator as a function of frequency and bias voltage in the vicinity of the superconducting gap $2\Delta/e$. The power of the probe tone is sufficiently low (-142 dBm) to keep the resonator population below 0.02 in order to be in the linear regime, where the measured spectrum is power independent. Below $375 \mu\text{V}$, the reflection coefficient S_{11} exhibits a resonance around $\omega/2\pi = 5.525 \text{ GHz}$ with a small dissipative response (-2 dB dip; see inset), indicating that the internal losses of the resonator are small, about $0.13\kappa_c$, as desired. When the voltage increases and reaches $(2\Delta - \hbar\omega)/e \approx 379 \mu\text{V}$, photons are absorbed by the junction through photon-assisted electron tunneling. The reflection dip correspondingly becomes more pronounced [inset, Fig. 2(a)]. Additionally, the resonance frequency shifts [dotted-dashed green line in Fig. 2(a)] due to the coupling to the junction, illustrating Kramers-Kronig relations [17,18,34]. At a given voltage, we fit the reflection S_{11} using

$$S_{11} = 1 - \frac{\kappa_c}{\kappa/2 + \kappa_c/2 + i\delta}, \quad (2)$$

where δ is the detuning between the source and the resonance frequency of the mode ω , which we fit together with κ_c and κ . The loss rate κ is the sum of the PAT loss rate κ_j and other intrinsic losses with a rate κ_i . We determine $\kappa_i = 2\pi \times 9.5 \text{ MHz}$ by taking the averaged value of κ below $340 \mu\text{V}$, where $\kappa_j \approx 0$. We then assume that κ_i is voltage independent and obtain $\kappa_j = \kappa - \kappa_i$. The evolution of κ_c and κ_j as a function of voltage is shown in the inset of

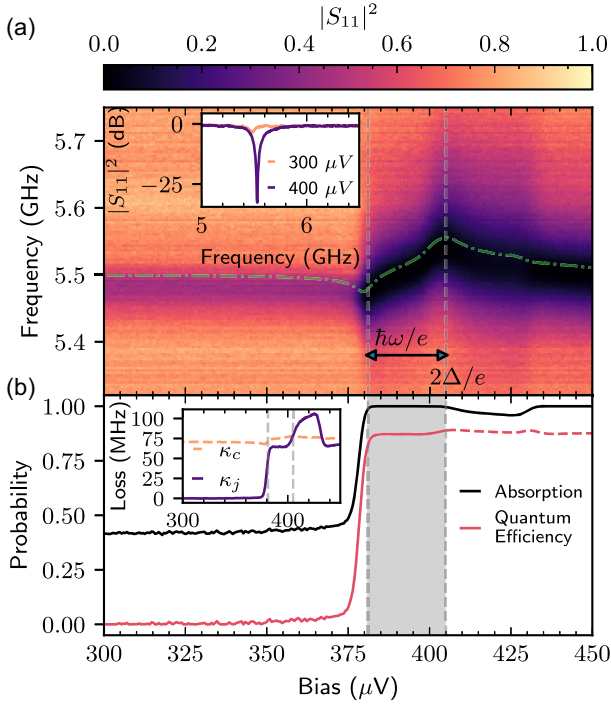


FIG. 2. Microwave spectroscopy. (a) Squared modulus $|S_{11}|^2$ of the microwave reflection coefficient near resonance vs frequency and bias voltage. The resonance frequency is shown as a green dash-dotted line and undergoes Lamb shift. Inset: frequency line cuts for two significant voltages (reference and critical coupling spectra). (b) Microwave absorption and expected quantum efficiency of photon-to-electron conversion deduced from the spectroscopic measurements shown in (a). The quantum efficiency is meaningful only for $eV < 2\Delta$, where elastic tunneling is negligible. Inset: voltage bias dependence of the coupling and junction induced loss rates κ_c and κ_j .

Fig. 2(b). The coupling rate κ_c only weakly depends on bias and is equal on average to $2\pi \times 75$ MHz in the range $2\Delta - \hbar\omega < eV < 2\Delta$, where the junction loss rate κ_j reaches $2\pi \times 65$ MHz in good agreement with (1) [38]. Above the gap, the elastic quasiparticle current leads to an out-of-equilibrium electronic distribution, which increases κ . When eV becomes larger than $2\Delta + \hbar\omega$, κ decreases abruptly as a consequence of photon emission by the junction into the resonator through inelastic tunneling.

From these values, we compute the probability that an incoming photon at resonance is absorbed $1 - |S_{11}|^2 = 1 - (\kappa - \kappa_c)^2 / (\kappa + \kappa_c)^2$ [see Fig. 2(b)]. Critical coupling, which corresponds to perfect absorption ($|S_{11}|^2 = 0$), is reached when $\kappa_j = \kappa_c - \kappa_i$. We observe a minimal reflection below -30 dB at the corresponding voltage [inset, Fig. 2(a)]. We can estimate the quantum efficiency by noting that the resonator population at resonance is $n_{\text{ph}} = 4\phi\kappa_c / (\kappa_c + \kappa)^2$, where ϕ is the incoming photon flux, which is proportional to the incident power P through $\phi = P/\hbar\omega$. The quantum efficiency is then $\kappa_j n_{\text{ph}} / \phi = 4\kappa_j \kappa_c / (\kappa_c + \kappa)^2$, which we also plot in Fig. 2(b). It is

maximal when $\kappa_j = \kappa_c + \kappa_i$, which happens at a voltage slightly above critical coupling. The expected efficiency is steadily around 87% over the full working window $2\Delta - \hbar\omega < eV < 2\Delta$ of the detector (gray area).

Photon-assisted tunneling current from coherent source—In order to verify that the losses induced by the junction indeed correspond to the conversion of photons into electrons, we measure the PAT current I_{PAT} as a function of the incident microwave power. Figure 3(a) shows the power dependence of the current-voltage characteristics when shining a microwave tone at the resonator frequency. As the power increases, a first subgap current step emerges that grows linearly with power. Additional steps appear at higher power that correspond to multi-photon absorption processes. Because of energy conservation, processes where N photons are absorbed to photo-assist the tunneling of one electron are allowed when $eV > 2\Delta - N\hbar\omega$. The colored bands indicate the process with minimal N allowed at each step. We measure the photocurrent at the center of the first four steps and plot their evolution with power in Fig. 3(b). The plotted I_{PAT} corresponds to the difference between the current with and without microwaves, not taking into account the dark current, which will be addressed later. At the $N = 1$ step, the ratio between I_{PAT}/e and the photon flux, is the quantum efficiency χ .

A precise direct measurement of χ is known to be difficult because of the unavoidable uncertainty on the value of the attenuation between the microwave source and the sample in the cryostat. In the limit $n_{\text{ph}} \ll 1$, the PAT current at step N is given by the population in the N Fock state multiplied by the rate $|\langle 0|D_\lambda|N\rangle|^2 \times I(V_m)/e$, where $V_m = (2\Delta + \hbar\omega/2)/e$. The population is given by $(\phi/\kappa_N)^N$, where κ_N is an effective loss rate, which depends on $\kappa_c, \kappa, \lambda$, and $I(V)$ and can be calculated analytically [38].

Fixing κ_c to $2\pi \times 75$ MHz, $\lambda = 0.79$, and using the independently measured resistance of the junction to estimate $I(V_m) = 190$ pA, the four I_{PAT} curves can be fitted with the attenuation as a single free parameter, which is very constrained because each curve is proportional to the N th power of the attenuation. Because the assumption $n_{\text{ph}} \ll 1$ rapidly breaks down with increasing power, the fitting procedure is a bit more elaborate and relies on the numerical simulation of the Lindblad master equation describing the dynamics of the resonator mode instead of the analytical expressions [38]. We obtain an attenuation of $-107.0(3)$ dB, corresponding to $\chi = 83\%$. The resulting simulated I_{PAT} curves are shown as solid lines in Fig. 3(b). The good quality of the fit for all the steps at once with a single adjustable parameter confirms our good understanding of the PAT processes. We estimate the systematic uncertainty on the quantum efficiency to be on the order of 0.05.

The deduced attenuation factor is only 1.0 dB above the estimated value that we obtain from an independent

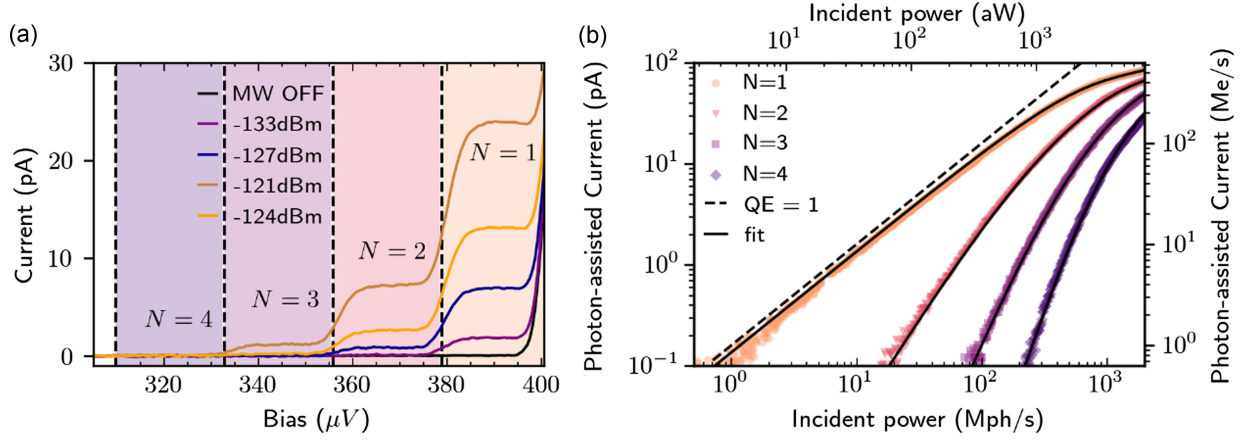


FIG. 3. Photon-assisted current and quantum efficiency. (a) Voltage dependence of the subgap current for different microwave powers at frequency $\omega/2\pi = 5.525$ GHz. At low power, a single step is observed when $2\Delta - \hbar\omega < eV < 2\Delta$ corresponding to a PAT current where one photon gives one electron. At higher powers, multiphoton processes involving the tunneling of a single electron with N absorbed photons occur when $eV > 2\Delta - N\hbar\omega$. (b) Power dependence of the $N = 1, 2, 3, 4$ PAT current steps and the corresponding theoretical prediction [38].

measurement of the overall transmission of the microwave lines of the cryostat and 0.2 dB above the one obtained by shot-noise calibration [38]. At large power, the detector saturates when n_{ph} becomes on the order of unity and multiphoton processes cannot be neglected. More specifically the 1 dB (3 dB) compression points occur respectively for $P = -119.0(-114.2)$ dBm or $\phi = 0.34(1.0)$ Gph/s.

Photon-assisted current from thermal population—As an independent test of our estimate of the quantum efficiency, we measure the conversion of the blackbody radiation coming from the matched $50\ \Omega$ load that is connected to the circulator port in direct view of the detector (see detailed circuit in [38]). We suppose that the load is thermalized to the fridge temperature. In the limit $n_{\text{ph}} \ll 1$, the expected equilibrium resonator population reads $n_{\text{ph}}(T) = (\kappa_c + \kappa_i) / (\kappa_c + \kappa_i + \kappa_j)n_{\text{BE}}(T)$ with the Bose-Einstein distribution $n_{\text{BE}}(T) = 1/[\exp(\hbar\omega/k_B T) - 1]$. This assumes that the coupling and intrinsic loss channels both connect the resonator to a bath at temperature T and that the junction behaves as a zero temperature bath. The corresponding thermally photon-assisted current is $e\kappa_j n_{\text{ph}}$. Here, we measure the total current, which is given by $I_D + e\kappa_j n_{\text{ph}}$, where I_D is the dark current of our detector. Figure 4 shows the measured current-voltage traces (inset) and the current at fixed bias voltage in the middle of the $N = 1$ step as a function of temperature from 20 to 150 mK. The full line corresponds to the expected current including a dark current $I_D = 55$ fA, while the dashed line shows the expected photocurrent $e\kappa_j n_{\text{ph}}$ alone. Again, the agreement between the simple prediction using the loss rates obtained from the resonator spectroscopy and the measured current is good without any adjustable parameters. The small discrepancy is explained if we consider the sample temperature to be 3 mK above the one measured by the thermometer. The voltage

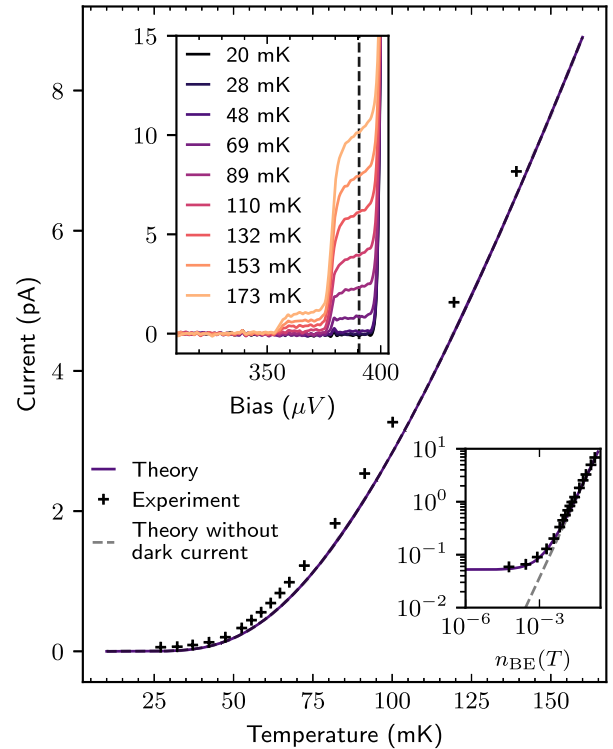


FIG. 4. Thermal photon-assisted current and dark current. Temperature dependence of the current measured at the center of the $N = 1$ photo-current step (dashed line in top inset). The full line is the expected current using the values of the loss rates fitted in Fig. 1 to which is added the measured dark current. The dashed line assumes zero dark current. Top inset: voltage dependence of the subgap current for different temperatures. Lower inset: same data as main in logarithmic scale vs $n_{\text{BE}}(T)$. The saturation at low temperature is due to the dark current of our detector.

dependence of the dark current (see Ref. [38]) indicates that it is not due to a rounding of the $I(V)$ of the junction near the gap but rather to a nonequilibrium population of the resonator mode that we estimate to $n_{\text{ph}} = 10^{-3}$, which corresponds to a temperature of 40 mK, close to the fridge temperature. We expect that a better shielding and filtering of the setup should reduce this value [7].

Noise equivalent power—In the data presented here, the current is measured using a differential voltage amplifier on a 51.6 k Ω resistor in series with the junction. The equivalent current noise of this setup is 120 fA/ $\sqrt{\text{Hz}}$, which results in a noise equivalent power of 3.3×10^{-18} W/ $\sqrt{\text{Hz}}$. The setup could be modified in order to reduce the current noise measurement to $\delta I = 1$ fA/ $\sqrt{\text{Hz}}$ by using a HEMT voltage amplifier [42] and increasing the value of the resistor in series with the junction, reducing the noise equivalent power to 3×10^{-20} W/ $\sqrt{\text{Hz}}$ on par with bolometric detection [43].

Conclusion—We have realized an important proof of concept regarding continuous and efficient low energy microwave photon-to-electron conversion using a high-impedance quantum circuit. The quantum efficiency of the process is unprecedentedly high (83%) compared to the state of the art [10] and is limited by the internal quality of the grAl resonator, which has been shown by others to be high [23]. The relatively large intrinsic losses of the sample are of unknown origin. Other resonators fabricated with the same technique have shown significantly larger intrinsic quality factors (about 2 times). Quantum efficiency as large as 99% should be within reach of this technique by increasing the intrinsic quality factor above 10^4 . We anticipate direct application to single microwave photon detection using quantum tunneling in a localized dot [9–13], in which the charge can be probed in real time [13] with a radio-frequency single electron transistor [44]. Given the charge sensitivity of state-of-the-art single electron transistor, single photons could be measured at a maximal rate of 100 kph/s. This will require one to lower the detection bandwidth (κ_c). The recent work in [7] shows that dark count rates as low as 100 Hz can be reached in a narrow band detector. Compared to superconducting qubit based detectors, continuous operation is possible and does not require high frequency pump signals. Also, qubit based detectors, though very efficient, can only be used in the photon counting regime and are intrinsically limited to low photon fluxes ($< \sim 100$ kph/s). Our detector can handle large fluxes and performs better than an ideal power detector behind a Josephson parametric amplifier with a noise temperature of one photon when the measurement bandwidth is larger than $\delta I^2 / (\eta e)^2 \simeq 50$ MHz. Finally, the very same detector, here demonstrated around 6 GHz, could be used at frequencies as high as twice the superconducting gap (≈ 100 GHz) by tuning the resonator dimensions. This could be of interest to axion search [45,46].

Acknowledgments—We thank R. Deblock, C. Quay Huei Li, A. Palacio-Morales for stimulating discussions,

C. Di Giorgio for her help in cabling the dilution fridge, L. Galvao-Tizei for TEM images. We acknowledge financial support from the ANR (ANR-21-CE47-0010 KIMIDET project and ANR-18-CE47-0003 BOCA project), from the France 2030 plan under the ANR-22-PETQ-0003 RobustSuperQ grant, from the Région Ile-de-France in the framework of DIM SIRTEQ (Science et Ingénierie en Région Ile-de-France pour les Technologies Quantiques) and the Laboratoire d'excellence Physique Atomes Lumière Matière (ANR-10-LABX-0039-PALM). This work was carried out as part of the NanoLPS micro-nanotechnology platform of the french RENATECH+ network.

- [1] M. D. Eisaman, J. Fan, A. Migdall, and S. V. Polyakov, Invited review article: Single-photon sources and detectors, *Rev. Sci. Instrum.* **82**, 071101 (2011).
- [2] S. R. Sathyamoorthy, T. M. Stace, and G. Johansson, Detecting itinerant single microwave photons, *C. R. Phys.* **Tome 17**, 756 (2016).
- [3] K. Inomata, Z. Lin, K. Koshino, W. D. Oliver, J.-S. Tsai, T. Yamamoto, and Y. Nakamura, Single microwave-photon detector using an artificial Λ -type three-level system, *Nat. Commun.* **7**, 12303 (2016).
- [4] J.-C. Besse, S. Gasparinetti, M. C. Collodo, T. Walter, P. Kurpiers, M. Pechal, C. Eichler, and A. Wallraff, Single-shot quantum nondemolition detection of individual itinerant microwave photons, *Phys. Rev. X* **8**, 021003 (2018).
- [5] R. Lescanne, S. Deléglise, E. Albertinale, U. Réglade, T. Capelle, E. Ivanov, T. Jacqmin, Z. Leghtas, and E. Flurin, Irreversible qubit-photon coupling for the detection of itinerant microwave photons, *Phys. Rev. X* **10**, 021038 (2020).
- [6] A. Blais, A. L. Grimsmo, S. M. Girvin, and A. Wallraff, Circuit quantum electrodynamics, *Rev. Mod. Phys.* **93**, 025005 (2021).
- [7] E. Albertinale, L. Balembois, E. Billaud, V. Ranjan, D. Flanigan, T. Schenkel, D. Estève, D. Vion, P. Bertet, and E. Flurin, Detecting spins by their fluorescence with a microwave photon counter, *Nature (London)* **600**, 434 (2021).
- [8] Z. Wang, L. Balembois, M. Rančić *et al.*, Single-electron spin resonance detection by microwave photon counting, *Nature (London)* **619**, 276 (2023).
- [9] C. H. Wong and M. G. Vavilov, Quantum efficiency of a single microwave photon detector based on a semiconductor double quantum dot, *Phys. Rev. A* **95**, 012325 (2017).
- [10] W. Khan, P. P. Potts, S. Lehmann, C. Thelander, K. A. Dick, P. Samuelsson, and V. F. Maisi, Efficient and continuous microwave photoconversion in hybrid cavity-semiconductor nanowire double quantum dot diodes, *Nat. Commun.* **12**, 5130 (2021).
- [11] S. Cornia *et al.*, Calibration-free and high-sensitivity microwave detectors based on InAs/InP nanowire double quantum dots, *Adv. Funct. Mater.* **33**, 2212517 (2023).
- [12] S. Haldar, D. Zenelaj, P. P. Potts, H. Havar, S. Lehmann, K. A. Dick, P. Samuelsson, and V. F. Maisi, Microwave power harvesting using resonator-coupled double quantum dot photodiode, *Phys. Rev. B* **109**, L081403 (2024).
- [13] S. Haldar *et al.*, Continuous microwave photon counting by semiconductor-superconductor hybrids, [arXiv:2401.06617](https://arxiv.org/abs/2401.06617).

- [14] A. H. Dayem and R. J. Martin, Quantum interaction of microwave radiation with tunneling between superconductors, *Phys. Rev. Lett.* **8**, 246 (1962).
- [15] P. K. Tien and J. P. Gordon, Multiphoton process observed in the interaction of microwave fields with the tunneling between superconductor films, *Phys. Rev.* **129**, 647 (1963).
- [16] J. R. Tucker and M. J. Feldman, Quantum detection at millimeter wavelengths, *Rev. Mod. Phys.* **57**, 1055 (1985).
- [17] A. H. Worsham, N. G. Ugras, D. Winkler, D. E. Prober, N. R. Erickson, and P. F. Goldsmith, Quantum tunneling currents in a superconducting junction, *Phys. Rev. Lett.* **67**, 3034 (1991).
- [18] J. Basset, H. Bouchiat, and R. Deblock, High-frequency quantum admittance and noise measurement with an on-chip resonant circuit, *Phys. Rev. B* **85**, 085435 (2012).
- [19] K. Tan, M. Partanen, R. E. Lake, J. Govenius, S. Masuda, and M. Möttönen, Quantum-circuit refrigerator, *Nat. Commun.* **8**, 15189 (2017).
- [20] A. Viitanen, T. Mörstedt, W. S. Teixeira, M. Tiiri, J. Rabinä, M. Silveri, and M. Möttönen, Quantum-circuit refrigeration of a superconducting microwave resonator well below a single quantum, *Phys. Rev. Res.* **6**, 023262 (2024).
- [21] A. J. Annunziata, D. F. Santavicca, L. Frunzio, G. Catelani, M. J. Rooks, A. Frydman, and D. E. Prober, Tunable superconducting nanoinductors, *Nanotechnology* **21**, 445202 (2010).
- [22] N. Samkharadze, A. Bruno, P. Scarlino, G. Zheng, D. P. DiVincenzo, L. DiCarlo, and L. M. K. Vandersypen, High-kinetic-inductance superconducting nanowire resonators for circuit QED in a magnetic field, *Phys. Rev. Appl.* **5**, 044004 (2016).
- [23] L. Grunhaupt, N. Maleeva, S. T. Skacel, M. Calvo, F. Levy-Bertrand, A. V. Ustinov, H. Rotzinger, A. Monfardini, G. Catelani, and I. M. Pop, Loss mechanisms and quasiparticle dynamics in superconducting microwave resonators made of thin-film granular aluminum, *Phys. Rev. Lett.* **121**, 117001 (2018).
- [24] N. Maleeva, T. Feo, T. Alan Harvey, and R. O. Prum, Circuit quantum electrodynamics of granular aluminum resonators, *Nat. Commun.* **9**, 1 (2018).
- [25] P. Kamenov, W.-S. Lu, K. Kalashnikov, T. DiNapoli, M. T. Bell, and M. E. Gershenson, Granular aluminum meandered superinductors for quantum circuits, *Phys. Rev. Appl.* **13**, 054051 (2020).
- [26] A. Glezer Moshe, E. Farber, and G. Deutscher, Granular superconductors for high kinetic inductance and low loss quantum devices, *Appl. Phys. Lett.* **117**, 062601 (2020).
- [27] Y.-F. Chen, D. Hover, S. Sendelbach, L. Maurer, S. T. Merkel, E. J. Pritchett, F. K. Wilhelm, and R. McDermott, Microwave photon counter based on Josephson junctions, *Phys. Rev. Lett.* **107**, 217401 (2011).
- [28] J. Leppäkangas, M. Marthaler, D. Hazra, S. Jebari, R. Albert, F. Blanchet, G. Johansson, and M. Hofheinz, Multiplying and detecting propagating microwave photons using inelastic Cooper-pair tunneling, *Phys. Rev. A* **97**, 013855 (2018).
- [29] S. Jebari, F. Blanchet, A. Grimm, D. Hazra, R. Albert, P. Joyez, D. Vion, D. Estève, F. Portier, and M. Hofheinz, Near-quantum-limited amplification from inelastic Cooper-pair tunnelling, *National electronics review* **1**, 223 (2018).
- [30] R. Albert, J. Griesmar, F. Blanchet, U. Martel, N. Bourlet, and M. Hofheinz, Microwave photon-number amplification, *Phys. Rev. X* **14**, 011011 (2024).
- [31] N. Crescini, S. Cailleaux, W. Guichard, C. Naud, O. Buisson, K. W. Murch, and N. Roch, Evidence of dual Shapiro steps in a Josephson junction array, *Nat. Phys.* **19**, 851 (2023).
- [32] N. Mehta, R. Kuzmin, C. Ciuti, and V. E. Manucharyan, Down-conversion of a single photon as a probe of many-body localization, *Nature (London)* **613**, 650 (2023).
- [33] J. Estève, M. Aprili, and J. Gabelli, Quantum dynamics of a microwave resonator strongly coupled to a tunnel junction, [arXiv:1807.02364](https://arxiv.org/abs/1807.02364).
- [34] G. Aiello *et al.*, Quantum bath engineering of a high impedance microwave mode through quasiparticle tunneling, *Nat. Commun.* **13**, 7146 (2023).
- [35] M. H. Devoret, D. Esteve, H. Grabert, G.-L. Ingold, H. Pothier, and C. Urbina, Effect of the electromagnetic environment on the Coulomb blockade in ultrasmall tunnel junctions, *Phys. Rev. Lett.* **64**, 1824 (1990).
- [36] *Single Charge Tunneling*, edited by H. Grabert and M. H. Devoret, NATO ASI Series B Vol. 294 (Plenum Press, New York, 1992), pp. 21–107.
- [37] J. R. Souquet, M. Woolley, J. Gabelli, P. Simon, and A. A. Clerk, Photon-assisted tunnelling with nonclassical light, *Nat. Commun.* **5**, 5562 (2014).
- [38] See Supplemental Material at <http://link.aps.org/supplemental/10.1103/PhysRevLett.133.076302>, which includes Refs. [39–41], and provide details about sample fabrication, experimental setup and theoretical calculations.
- [39] K. E. Cahill and R. J. Glauber, Ordered expansions in boson amplitude operators, *Phys. Rev.* **177**, 1857 (1969).
- [40] G. C. Ménard, A. Peugeot, C. Padurariu, C. Rolland, B. Kubala, Y. Mukharsky, Z. Iftikhar, C. Altimiras, P. Roche, H. Le Sueur, P. Joyez, D. Vion, D. Esteve, J. Ankerhold, and F. Portier, Emission of photon multiplets by a dc-biased superconducting circuit, *Phys. Rev. X* **12**, 021006 (2022).
- [41] J. R. Johansson, P. D. Nation, and F. Nori, QUTIP2: A Python framework for the dynamics of open quantum systems, *Comput. Phys. Commun.* **184**, 1234 (2013).
- [42] Y. Jin *et al.*, Ultra-low noise CryoHEMTs for cryogenic high-impedance readout electronics: Results and applications, *Proceedings of the 13th IEEE International Conference on Solid-State and Integrated Circuit Technology (ICSICT), Hangzhou, China, 2016* (IEEE, New York, 2016), pp. 342–345, [10.1109/ICSICT.2016.7998915](https://doi.org/10.1109/ICSICT.2016.7998915).
- [43] R. Kokkonen *et al.*, Bolometer operating at the threshold for circuit quantum electrodynamics, *Nature (London)* **586**, 47 (2020).
- [44] R. J. Schoelkopf, P. Wahlgren, A. A. Kozhevnikov, P. Delsing, and D. E. Prober, The radio-frequency single-electron transistor (RF-SET): A fast and ultrasensitive electrometer, *Science* **280**, 1238 (1998).
- [45] P. Sikivie, Invisible axion search methods, *Rev. Mod. Phys.* **93**, 015004 (2021).
- [46] A. L. Pankratov, L. S. Revin, A. V. Gordeeva, A. A. Yablokov, L. S. Kuzmin, and E. Il'ichev, Towards a microwave single-photon counter for searching axions, *npj Quantum Inf.* **8**, 61 (2022).